

RESEARCH ARTICLE

10.1029/2018JA025292

Special Section:

Dayside Magnetosphere Interaction

Key Points:

- Identification of the current carriers and sources within the magnetopause boundary layer is made
- The ion diamagnetic current is found to be the main source of the perpendicular current
- Two-fluid MHD theory is shown to hold for an ion gyroradius scale boundary layer, while it is partly violated for a more complex structure

Correspondence to:

M. W. Dunlop,
malcolm.dunlop@stfc.ac.uk

Citation:

Dong, X.-C., Dunlop, M. W., Wang, T.-Y., Cao, J.-B., Trattner, K. J., Bamford, R., et al. (2018). Carriers and sources of magnetopause current: MMS case study. *Journal of Geophysical Research: Space Physics*, 123, 5464–5475. <https://doi.org/10.1029/2018JA025292>

Received 31 JAN 2018

Accepted 22 JUN 2018

Accepted article online 3 JUL 2018

Published online 17 JUL 2018

Carriers and Sources of Magnetopause Current: MMS Case Study

X.-C. Dong¹ , M. W. Dunlop^{1,2} , T.-Y. Wang² , J.-B. Cao¹ , K. J. Trattner³ , R. Bamford², C. T. Russell⁴ , R. Bingham² , R. J. Strangeway⁴ , R. C. Fear⁵ , B. L. Giles⁶ , and R. B. Torbert^{7,8} 

¹School of Space and Environment, Beihang University, Beijing, China, ²RAL Space, STFC, Oxfordshire, UK, ³LASP University of Colorado, Boulder, CO, USA, ⁴Department of Earth, Planetary and Space Sciences, UCLA, Los Angeles, CA, USA, ⁵Department of Physics and Astronomy, University of Southampton, Southampton, UK, ⁶NASA Goddard Space Flight Center, Greenbelt, MD, USA, ⁷Institute for the Study of Earth, Oceans, and Space, University of New Hampshire, Durham, NH, USA, ⁸Southwest Research Institute, San Antonio, TX, USA

Abstract We investigate the current carriers and current sources of an ion scale tangential magnetopause current layer using the Magnetospheric Multiscale four spacecraft data. Within this magnetopause current layer, ions and electrons equally contribute to the perpendicular current, while electrons carry nearly all the parallel current. The energy range of all these current carriers is predominantly from middle to high (>100 eV), where particles with higher energies are more efficient in producing the current. By comparing each term, two-fluid magnetohydrodynamic (MHD) theory is able to describe the current sources to a large degree because the sum of all the perpendicular currents from MHD theory could account for the currents observed. In addition, we find that the ion diamagnetic current is the main source of the total perpendicular current, while the curvature current can be neglected. Nevertheless, ions and electrons both carry comparable current due to the redistribution of the electric field and show features beyond the classic Chapman-Ferraro model, particularly on the front side of the boundary layer where the electric field reversal is most intense. We also show a second, comparative event in which ions do not satisfy MHD theory, while the electrons do. The small-scale, adiabatic parameter (square of curvature radius/gyroradius) supports our interpretation that this second event contains ion scale substructure. We suggest that comparing the predicted MHD current with plasma current can be a good method to judge whether the MHD theory is satisfied in each specific circumstance, especially for high-precision Magnetospheric Multiscale data.

1. Introduction

The Earth's magnetopause (MP) is a key region for the transfer of mass, momentum, and energy from the solar wind into the magnetosphere (MSP). Typically, a current layer exists between the Earth's magnetospheric field and the shocked solar wind (in the magnetosheath [MSH]). Similar to the current sheet in the magnetospheric tail, a basic plasma process, magnetic reconnection, occurs in this current layer (e.g., Dong et al., 2017; Dunlop et al., 2011; Phan et al., 2004; Trenchi et al., 2008), which plays an important role in the whole magnetospheric dynamics. This current layer is thus a key region to investigate the physical processes at the MP.

Although the MP has been extensively studied for many years, direct measurement of the vector current density has not been possible until the four spacecraft Cluster mission. Based on the curlometer method (Dunlop et al., 2002), the large-scale features of MP current layer have been revealed using the Cluster observations (e.g., Dunlop & Balogh, 2005; Haaland et al., 2004, 2014; Panov et al., 2011), typically for MP with thicknesses down to a few hundred kilometers. The scale size of the Cluster configuration and the low cadence of the plasma moments limited the spatial resolution achievable with Cluster (Dunlop et al., 2016). The Magnetospheric Multiscale (MMS) mission (Burch et al., 2015), with four spacecraft at smaller separation distances (a few to tens of kilometers), now provides high precision and high cadence plasma data, which enables the intimate detail of the current layer to be probed, as well as the current carriers to be tracked.

While a basic question is what physical processes operate in the MP current layer, our knowledge about it remains incomplete. The classical closed MP has often been considered as a simple current layer (e.g., as in the Chapman-Ferraro model; Chapman & Ferraro, 1930), where the current is created by the opposite

motion of electrons and ions as they encounter the magnetospheric dipole magnetic field at the boundary. According to this concept, the current layer thickness should be an ion gyration radius or less because an electric field is set up by charge separation; however, this induces finite gyroradius effects so that the concept is not fully self-consistent. Previous statistical results indicate that the average thickness of the dayside MP current layer is about 900 km near subsolar region (e.g., Berchem & Russell, 1982; Le & Russell, 1994) and 1,500 km at flank side (Haaland et al., 2014). These results indicate that the ideal Chapman-Ferraro model cannot fully explain the morphology of the actual MP current layer. At the real MP, particles may not return to the MSH but can become trapped and move along the boundary. Nevertheless, these particles could be treated as fluid population and described by MHD theory.

According to multifluid MHD theory, the stationary drift velocity of the s component fluid, as derived from momentum conservation equation, is (e.g., Baumjohann & Treumann, 1997)

$$\mathbf{v}_s = \frac{\mathbf{E} \times \mathbf{B}}{B^2} + \frac{1}{q_s n_s B^2} \mathbf{B} \times \nabla p_{s\perp} + \frac{1}{q_s n_s B^2} \mathbf{B} \times \nabla \cdot \left[(p_{s\parallel} - p_{s\perp}) \frac{\mathbf{B}\mathbf{B}}{B^2} \right] \quad (1)$$

where \mathbf{E} , \mathbf{B} , n_s are electric field, magnetic field, and density of the s component fluid, respectively. $p_{s\parallel}$ ($p_{s\perp}$) is the plasma pressure along (across) \mathbf{B} .

Then the current density of the s component fluid is

$$\mathbf{j}_{\perp s} = q_s n_s \frac{\mathbf{E} \times \mathbf{B}}{B^2} + \frac{\mathbf{B} \times \nabla p_{s\perp}}{B^2} - \frac{p_{s\parallel} - p_{s\perp}}{B^2 R_c} \mathbf{B} \times \mathbf{n} \quad (2)$$

where the term $\nabla \cdot \frac{\mathbf{B}\mathbf{B}}{B^2}$ in equation (1) is replaced by using the fact that the derivative of a unit vector is equal to the outer normal, \mathbf{n} (the local curvature vector of the magnetic field), divided by R_c (the curvature radius). Equation (2) shows that perpendicular current of s component $\mathbf{j}_{\perp s}$ consists of a cross-field drift current ($\mathbf{j}_{\mathbf{E} \times \mathbf{B}}$), a diamagnetic drift current (\mathbf{j}_{dia}), and a curvature drift current ($\mathbf{j}_{\text{dia}, c}$), respectively.

When the spatial scales operating within the MP boundary layer are smaller than the ion gyroradius, ions will become demagnetized and therefore do not satisfy the MHD theory. Whether MHD theory can be used at the MP under various conditions is a question for concern.

In this paper, we use high precision MMS data to analyze current structure and plasma features associated with the current carriers during a thin, ion gyroradius scale, tangential-discontinuity MP crossing. In particular, we examine detailed particle species (i.e., ion and electron) and the energy ranges of the current carriers. We also calculate each term of equation (2) and try to use anisotropic MHD theory to explain the perpendicular current of this thin current layer. At the end, we show another event which does not satisfy the MHD theory and compare this event with the first one.

2. Observations

We use the magnetic field data from the fluxgate magnetometer (Russell et al., 2016), plasma data from the fast plasma investigation (Pollock et al., 2016) and electric field data from electric field double probes (Lindqvist et al., 2016). The electric current density is calculated from the curlometer and also directly from the plasma moments ($\mathbf{j} = q n_e (\mathbf{v}_i - \mathbf{v}_e)$) at each spacecraft. We also compare the mean of the plasma currents across all spacecraft positions with the curlometer current. Ion and electron currents are calculated from their velocity moments in the spacecraft frame, respectively (this is part of the MMS data product definition). Calculated results below show that the velocity of the MP current layer is perpendicular to its plane, indicating that the difference between the MP frame and the spacecraft frame does not affect the interpretation of the MP current analysis discussed here.

Using the above MMS data, we calculate the cross-field drift current $\mathbf{j}_{\mathbf{E} \times \mathbf{B}} = q_s n_s \frac{\mathbf{E} \times \mathbf{B}}{B^2}$ from the electric and magnetic field data and average over the four spacecraft. Because the four spacecraft generally form operational a well-defined tetrahedral shape, and all payload instruments have very high precision (30 ms for electron and 150 ms for ion) plasma data, we can also use multispacecraft methods to calculate the gradient of plasma pressure $\nabla p_{s\perp}$ (Paschmann & Schwartz, 2000), thereby obtaining the diamagnetic current $\mathbf{j}_{\text{dia}} = \frac{\mathbf{B} \times \nabla p_{s\perp}}{B^2}$. The curvature radius (R_c) and direction (\mathbf{n}) of magnetic field can be calculated

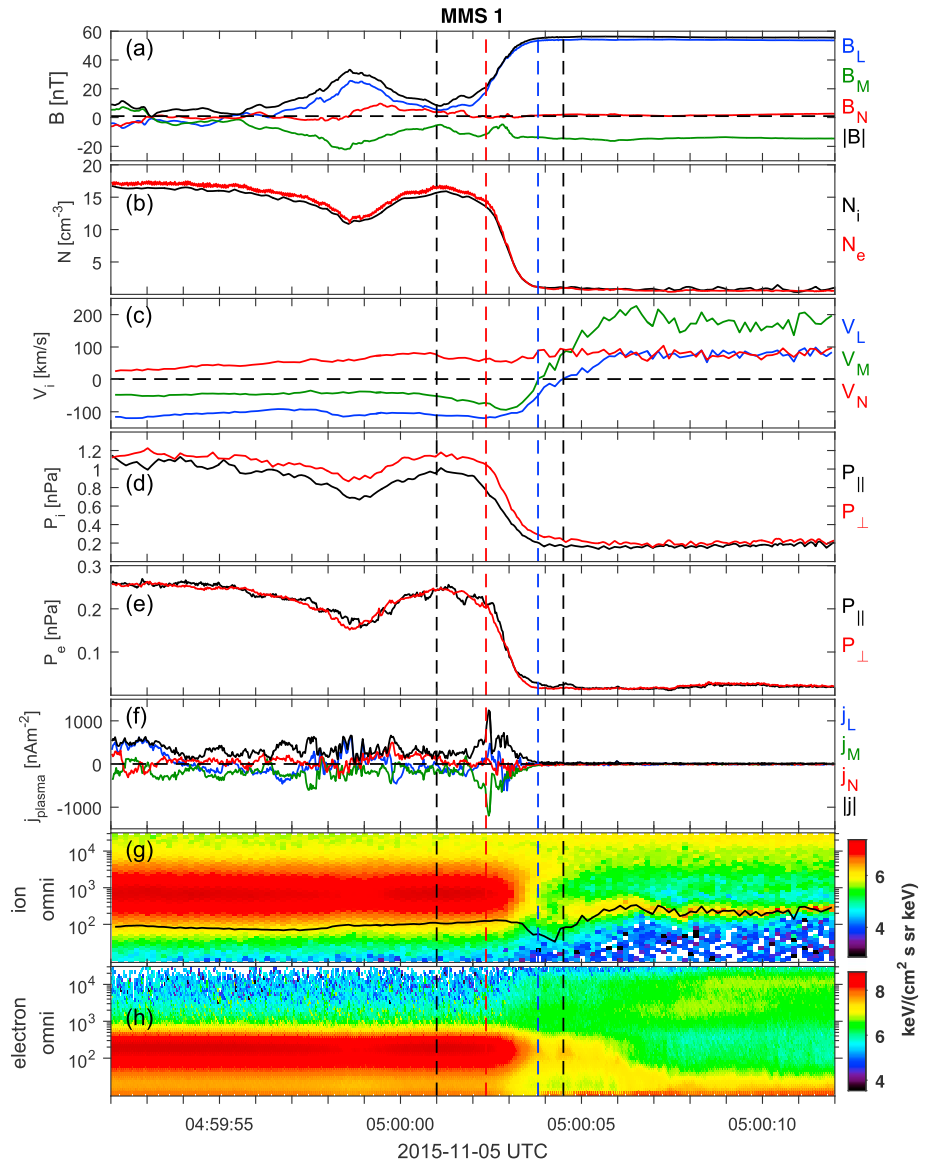


Figure 1. Overview of the magnetopause crossing observed by Magnetospheric Multiscale 1 on 5 November 2015. (a) The vector magnetic field, (b) the ion and electron densities, (c) the ion velocity, (d and e) the ion and electron pressure, (f) current from plasma moments, and (g and h) the electron and ion spectrograms of differential energy flux. The black line in (g) is the ion velocity magnitude. The interval between two black vertical dashed lines is the range which will be analyzed in detail. The red and blue dashed lines will be introduced in the next section.

by magnetic curvature analysis (Shen et al., 2003). Based on that, we can obtain the curvature drift current $\mathbf{j}_{\text{dia,c}} = -\frac{P_{\text{||}} - P_{\text{⊥}}}{B^2 R_c} \mathbf{B} \times \mathbf{n}$ using the anisotropic pressure measurement. Thus, all the terms in equation (2) can be calculated with MMS data.

2.1. Overview

We investigate the MP crossing observed on 5 November 2015 around 05:05:50 UT, where Figure 1 shows an overview of the MP crossing observed by MMS1. At this time the four spacecraft were in a regular tetrahedral configuration with an average separation of ~ 11 km. The spacecraft crossed the MP at [10.5, 2.1, -0.5] Earth radii in geocentric solar ecliptic coordinates. We transform all the vector data into LMN coordinates, based on minimum variance analysis of the magnetic field from MMS1 during the MP crossing. The LMN coordinates

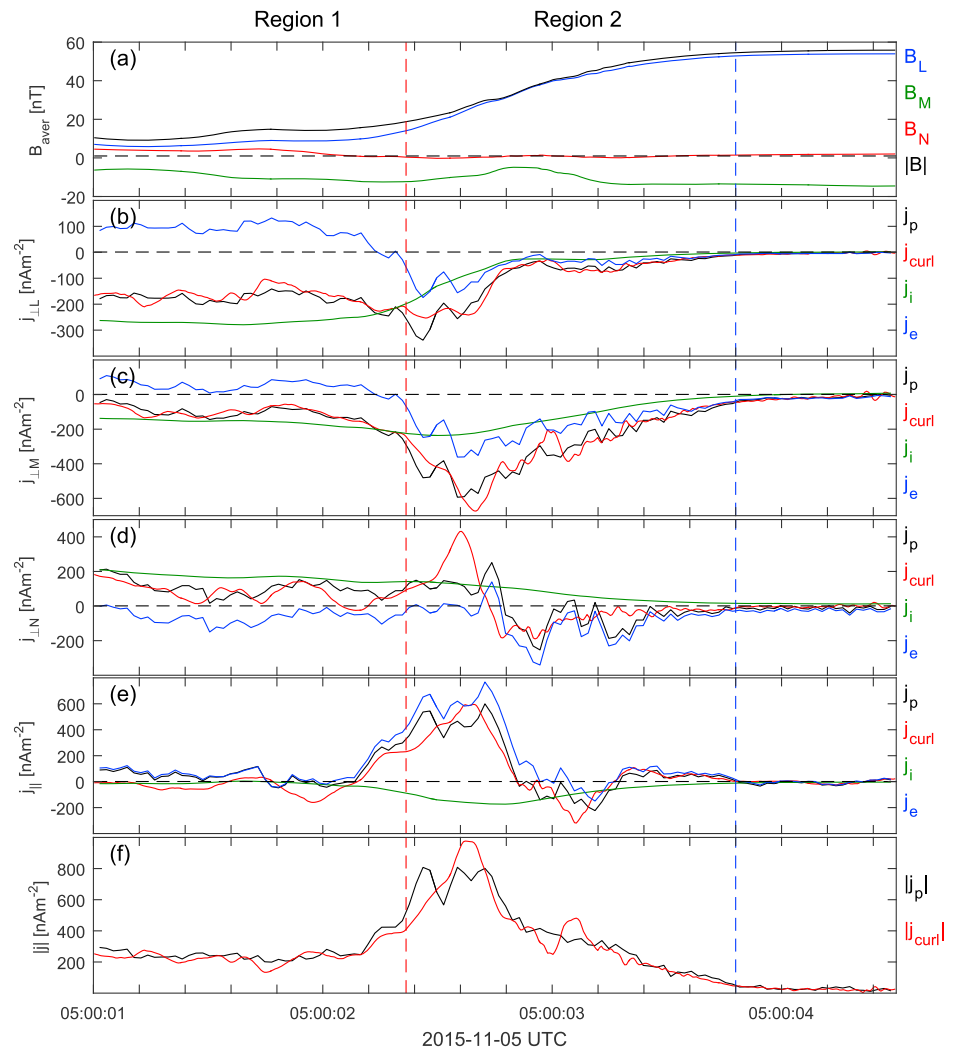


Figure 2. Electric current and current carriers of the magnetopause crossing. (a) The vector magnetic field, (b) perpendicular current from plasma moments (black), (c) curlometer (red), (d) ion current (green), electron current (blue), (e) parallel current from plasma moments and curlometer, and (f) total current magnitude from plasma moments and curlometer.

are $L = [0.27, -0.37, 0.89]$, $M = [0.09, -0.91, -0.41]$ (dawnward), and $N = [0.96, 0.19, -0.21]$ in geocentric solar ecliptic coordinates.

Magnetospheric Multiscale 1 was initially in the MSH, characterized by low magnitude magnetic field and cold and dense plasma ($>15 \text{ cm}^{-3}$) until a partial MP crossing from 04:59:56 to 05:00:01 UT (decrease of density and rotation of magnetic field to MP direction), then moved back to MSH again. Following this excursion MMS1 fully crossed the MP from 05:00:01 to 05:00:04.5 UT, accompanied by a strong current layer. In this range, the magnetic field strength increased from 9 to 56 nT and the plasma density decreased from 16 to below 1 cm^{-3} . We can also see a large decrease of ion and electron pressure (Figures 1d and 1e). The maximum magnitude of current reaches up to $1,200 \text{ nAm}^{-2}$ in this MP crossing (Figure 1f). The spacecraft then enter into the MSP, characterized by low density ($<1 \text{ cm}^{-3}$) and lack of broadband low energy distribution spectrum (Figures 1g and 1h).

There is a cold magnetospheric ion population in the MSP, seen as a narrow beam at $E \sim 250 \text{ eV}$ in Figure 1g after 05:00:04.5 UT. This population accounts for all the velocity moment in the MSP (Figure 1c and black line in Figure 1g). During the full MP crossing, the shear angle is $\sim 40^\circ$ and the change of ion plasma beta $\Delta\beta > 40$. These conditions suppress the onset of magnetic reconnection (Phan et al., 2010). We indeed do not observe

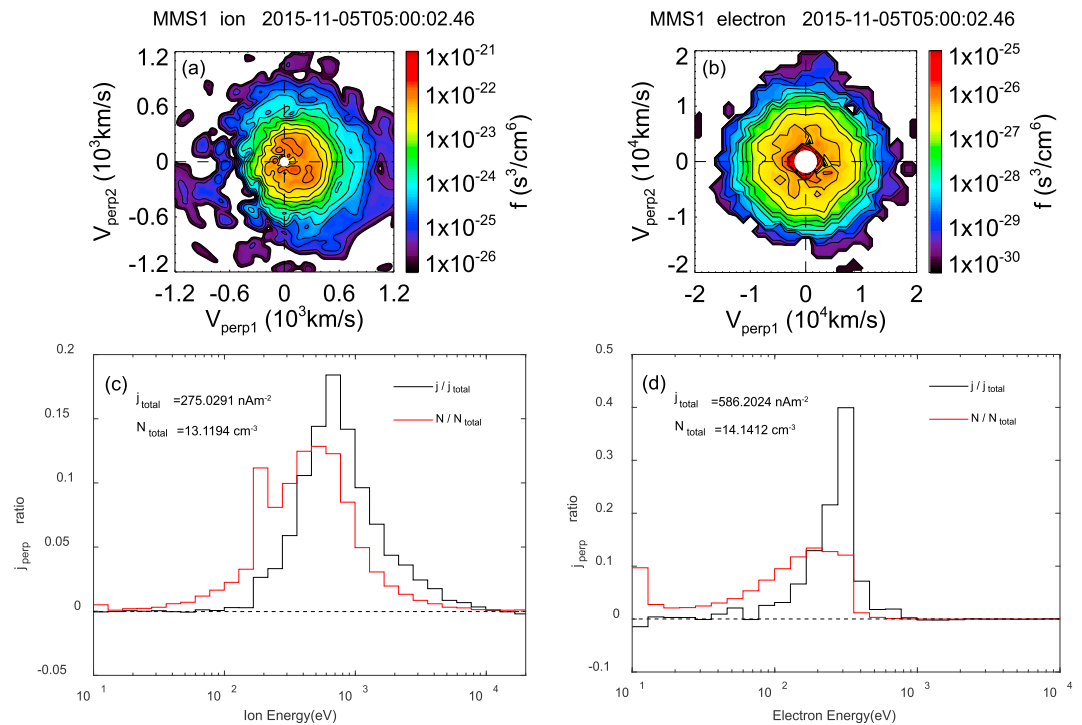


Figure 3. Plasma distribution and detailed current carrier at 05:00:02.6 UT. (a and b) Ion and electron velocity space distributions are shown in the plane normal to \mathbf{B} with the two orthogonal axes V_{perp1} and V_{perp2} . V_{perp1} is in the direction of $(\mathbf{b} \times \mathbf{v}) \times \mathbf{b}$, and V_{perp2} is along $-\mathbf{v} \times \mathbf{b}$ (\mathbf{b} and \mathbf{v} are the measured unit vectors of the magnetic field and velocity moment, respectively). (c and d) The black/red lines are the ratio of plasma current/density at each energy range to the total plasma current/density, for ions and electrons, respectively.

any reconnection jets and other reconnection features here. Using the timing method, we find that the first and second parts of this strong current region from 05:00:02 UT to 05:00:03.5 UT have two different velocities (49 and 67 km/s). The average velocity of the strong current region is 58 km/s, directed mainly in the N direction, and the width of the current layer is therefore 87 km. This width is a little larger than the ion gyroradius (the gyroradius of the 450-eV proton in the 55-nT magnetic field is 56 km, to be a typical example) and therefore is expected to be a well behaved example of conditions leading to a Chapman/Ferraro current layer.

2.2. Current and Current Carriers

Figure 2 shows the electric current and the contributions from each current carrier for this MP crossing. The plotted time range is the interval between two vertical black dashed lines in Figure 1. The black and red lines in Figures 2b–2f show that the total current densities derived from the curlometer and the corresponding high-resolution plasma data are broadly in close agreement, and this is true for both the perpendicular and the parallel currents separately, except for some small substructures, particularly near the front side of the MP boundary layer (after dashed red vertical line). The observed similarities certify the accuracy of the plasma data and show that the significant plasma current populations fall within the range of the fast plasma investigation instruments, which allows further analysis to be made by single spacecraft plasma data. The measured currents for ions and electrons separately are also shown.

We should note here the significance of the comparison of the curlometer estimates and the measured plasma currents shown in Figure 2. The plots show the plasma moments averaged over all MMS spacecraft. In principle, the currents can be calculated at each spacecraft in turn and indeed typically show differences in the signatures at each and therefore provide some information on the spatial structure of the current within the tetrahedron, limited to the cadence of the plasma moments. The current measured by the plasma moments reflects only the plasma populations with energies in the range of measured energies of the

plasma instruments, so that cold or very energetic particles will not contribute. In contrast the curlometer provides a linear estimate of the current from curl B on a spatial scale relevant to the volume of the MMS configuration, but only limited by the cadence of the magnetic field measurements. Thus, the curlometer provides an estimate of the mean current typically at a higher time resolution than the plasma currents, whereas the plasma estimates potentially show current structure across the MMS configuration, but only where the missed plasma populations are not significant to the current (see Dunlop et al., 2016 for further discussion).

We divide this interval into regions by the red and blue dashed lines. For the region before the red line (region 1), the total perpendicular current is dominated by ions, while the electron current is in the opposite direction (Figures 2b–2d). The current contribution from both ions and electrons is comparable in the region between the red and blue lines (region 2).

A strong field-aligned parallel current also exists in this current layer (Figure 2e), growing just before the dashed red line. This parallel current is positive initially and changes to negative in the center. The dominant carriers of this parallel current are electrons except for the small region when it turns negative.

2.2.1. Detailed Current Carrier of the Perpendicular Current

Figure 3 shows the ion and electron distributions and details of the current carriers at the time point when the current magnitude of MMS1 is the largest (Figure 1f). The plasma distributions shown are in the plane perpendicular to \mathbf{B} . We can see the clear nongyrotropic distribution for ions (Figure 3a), especially for the higher energies. This nongyrotropic distribution created the perpendicular ion velocity and current. The electron distribution is slightly nongyrotropic in the high-energy range (Figure 3b).

In order to analyze the current carriers quantitatively, we plot the detailed current created at each energy for electrons and ions separately (Figures 3c and 3d). The current is directly calculated from plasma density and velocity, which are integrated from distribution function data. The perpendicular ion current mainly arises from energies between 358 and 1,283 eV (72% current; Figure 3c), and when compared to the density profile, we see that the high-energy ions have more efficiency to generate the current (the black line is higher than the red line). From Figure 3d, one can clearly see that the electron current mainly arises from 166 to 358-eV electrons (74.5% current with 38.3% density). The higher-energy electrons have much more efficiency in generating the current, which is similar to the case of ions.

2.2.2. Detailed Current Carrier of the Parallel Current

Figure 4 shows the properties associated with the parallel current. Figure 4b reproduces the result from Figure 2, that the parallel current in the boundary layer is mainly in the positive direction but turns to negative for a while near the MSP side of the boundary layer. We find that electrons are the dominant current carriers, while ions offer a small background current during this interval. In order to analyze the detailed current carriers, we plot the logarithm ratio of parallel to antiparallel electron differential energy flux (Figure 4e). We can see that the middle energy (100–800 eV) electrons have a large ratio; the ratio is first positive (mainly in the parallel direction) and then becomes negative (mainly in the antiparallel direction) within the current region, suggesting that these electrons are the current carriers of the parallel/antiparallel current. We also plot the detailed current carriers of each energy range at two selected time points indicated by black arrows in Figure 4e (Figures 4f and 4g). It shows that the current carriers lie at energies larger than 100 eV which is indeed similar to the result from Figure 4e. The 128–357 eV electrons created 83.9% of the current with only 38.7% of the density shown in Figure 4f, while the current from the <100-eV electrons can be neglected.

2.3. Current Sources of the Perpendicular Current

In order to investigate the sources of the MP current and account for the ion/electron perpendicular response, we calculate each term in equation (2) to get the cross-field drift current ($\mathbf{j}_{\mathbf{E} \times \mathbf{B}}$), the diamagnetic drift current (\mathbf{j}_{dia}), and the curvature drift current ($\mathbf{j}_{\text{dia}, c}$), respectively. These results are shown in Figure 5. The vertical scales for the currents in each panel are the same. It needs to be mentioned that the calculated curvature radius R_c is very much larger than the MMS spatial scale, so the results from magnetic curvature analysis are reliable (Shen et al., 2003).

Figures 5b and 5c show that j_{dia} is broadly consistent with the total j_{\perp} except for some substructures. A key difference occurs particularly near the front side of the MP boundary layer (i.e., just after the dashed red line). Throughout this interval $j_{\text{dia}, c}$ is very small and can be neglected except for a short time in the MSH near

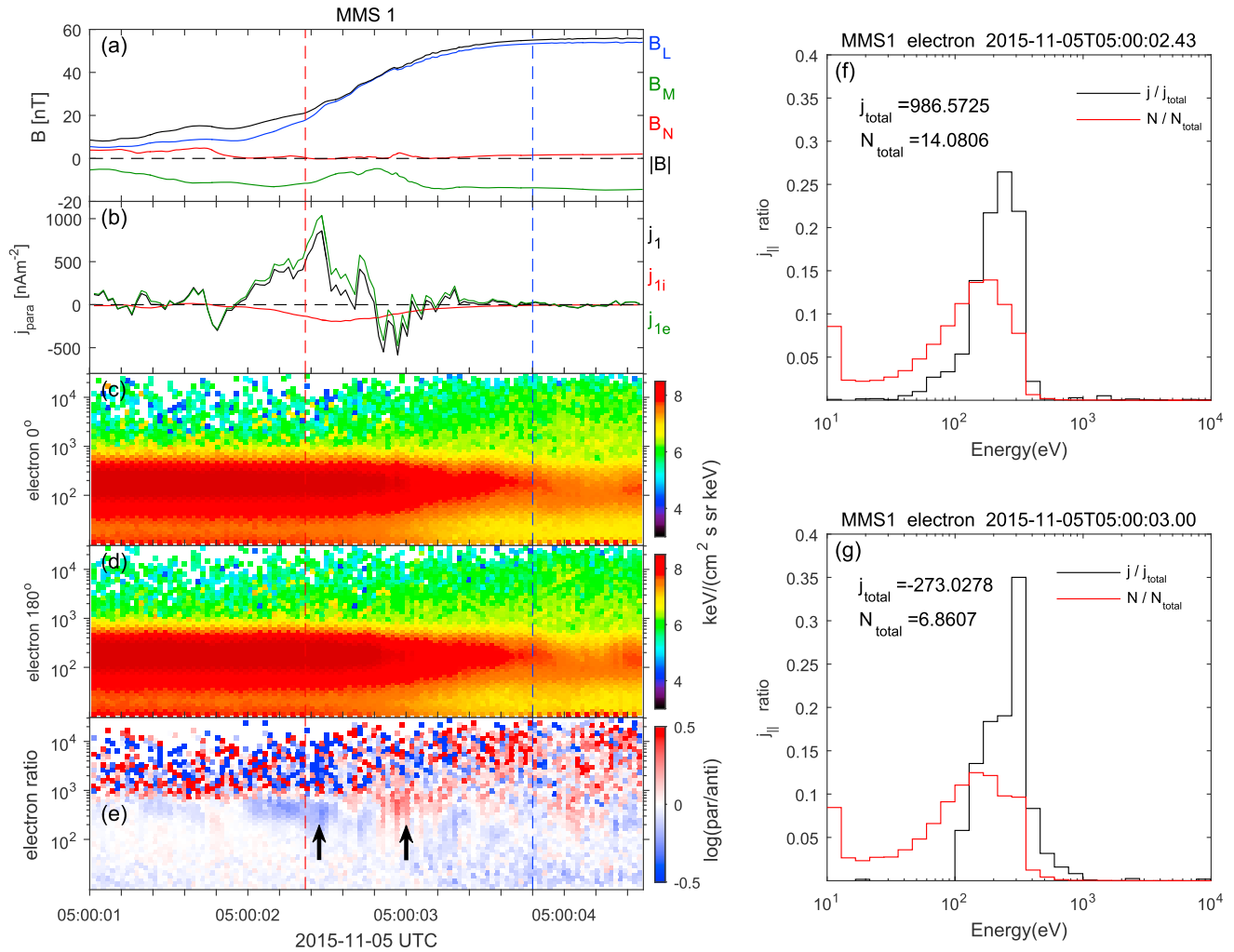


Figure 4. Parallel current carrier of Magnetospheric Multiscale 1 during the magnetopause crossing. (a) Magnetic field and (b) ion, electron, and total current. (c and d) Electron differential energy flux spectrogram in parallel/antiparallel direction, (e) the ratio of parallel and antiparallel electron differential energy fluxes, and (f and g) detailed current carrier of each energy range at the time points indicated by black arrows in (c).

05:00:01.3 UT. The small $j_{\text{dia}, c}$ may be caused by the small plasma anisotropy (Figures 1d and 1e) and relatively large curvature radius and is consistent with the events having an overall scale size larger than the ion gyroradius. The comparison of $j_{i, \text{dia}}$ and $j_{e, \text{dia}}$ in Figures 5d and 5e shows that the ion diamagnetic current, $j_{i, \text{dia}}$, contributes 85% to the total j_{dia} and that $j_{e, \text{dia}}$ accounts for the remaining 15% throughout regions 1 and 2. Thus, most of the current source is carried by the ions as reflected by $j_{i, \text{dia}}$.

As described before, ions and electrons contribute almost the same amount of perpendicular current in region 2 (Figures 2b–2d). However, Figure 5 shows that most of the source of the perpendicular current is $j_{i, \text{dia}}$. It is therefore apparent that $j_{e, \text{dia}}$ does not represent the full, measured electron perpendicular current $j_{e\perp}$ as shown in Figures 2b–2d. We calculate the ion and electron $j_{\text{dia}}, j_{E \times B}$ and $j_{E \times B + \text{dia}}$ and compare them with the calculated j_{\perp} (Figures 5f–5i). Indeed $j_{e, \text{dia}}$ deviates from $j_{e\perp}$ throughout. The lower panels in Figures 5f–5i show that this is in part accounted for by inclusion of the $\mathbf{E} \times \mathbf{B}$ perpendicular currents, since from equation (2), we can suppose that $j_{E \times B}$ may play a significant role.

In region 2, we find that $j_{i, \text{dia}}$ is larger than $j_{i\perp}$ initially, which is reduced by the small negative effect of $j_{i, E \times B}$. Thus, the total $j_{i, E \times B + \text{dia}}$ is consistent with $j_{i\perp}$ (Figures 5f and 5g). For the electrons, $j_{e, \text{dia}}$ is much less than $j_{e\perp}$ and the addition of $j_{e, E \times B}$ partially increases the electron current so that the total $j_{e, E \times B + \text{dia}}$ is almost consistent with $j_{e\perp}$, but only during the later time interval (Figures 5h and 5i). Thus, we can see that in the

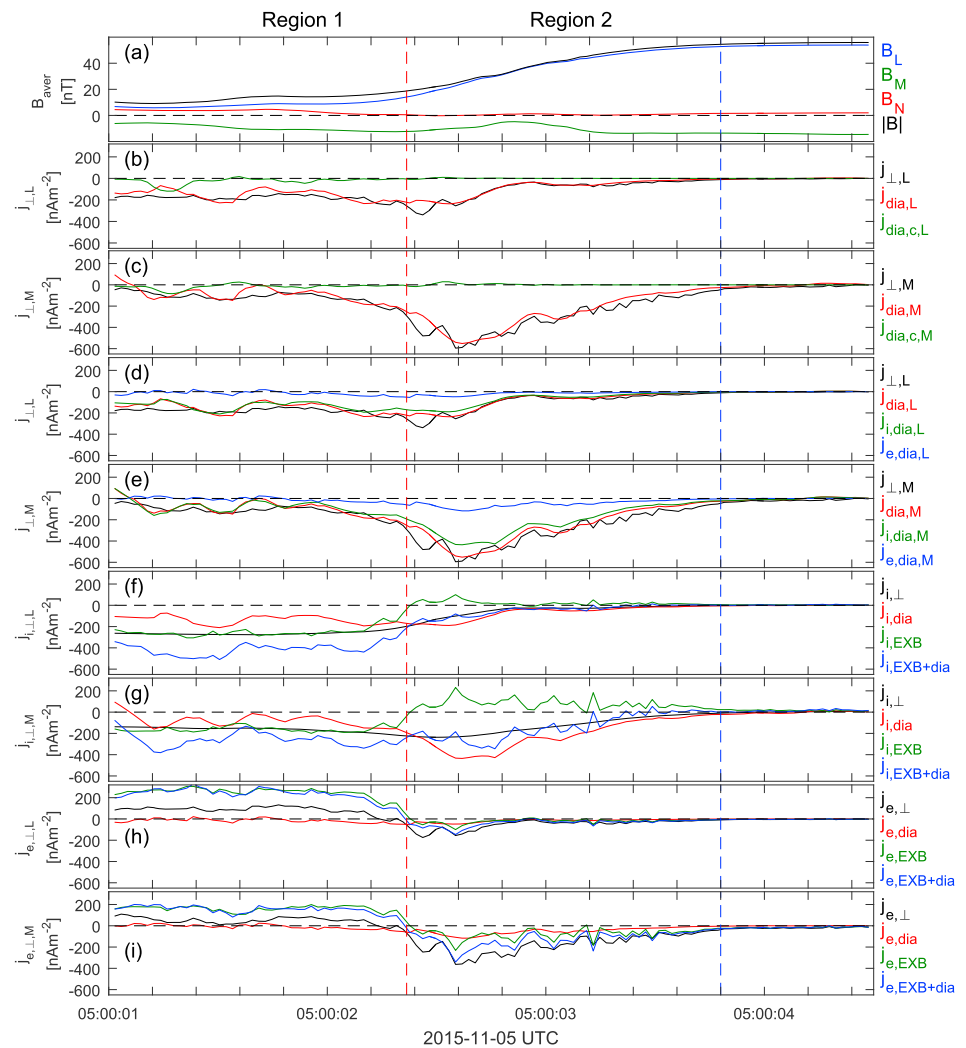


Figure 5. All the calculated terms in equation (2) on 5 November 2015. (a) Four spacecraft average magnetic field; (b and c) perpendicular current from four spacecraft plasma moments j_{\perp} (black), diamagnetic drift current j_{dia} (red), and curvature drift current $j_{\text{dia},c}$ (green); (d and e) perpendicular current j_{\perp} (black), diamagnetic drift current j_{dia} (red), and ion/electron diamagnetic drift current $j_{i,\text{dia}}$ (green)/ $j_{e,\text{dia}}$ (blue); (f–i) ion/electron perpendicular current (black), diamagnetic drift current (red), cross-field drift current (green), sum of diamagnetic drift current, and cross-field drift current (blue).

region near the front side of the region 2 the electron current is not consistent with $j_{e,E \times B + \text{dia}}$. This could suggest non-MHD behavior of electrons or at least deviations from the classical Chapman-Ferraro picture. We should note, however, that the first burst of electron perpendicular current in region 2 is not seen in the curlometer result, which tracks j_{dia} more closely. This would be consistent with the electron behavior being controlled by a very narrow region.

In region 1, $j_{i\perp}$ seems like represented by the $j_{i,E \times B}$. This is due to the fact that the accuracy of electric field is not high in this region. From Figures 5b and 5c, we find that the j_{dia} is consistent with j_{\perp} . This means that the j_{dia} result is reliable and is indeed the whole source of current. Because the terms $j_{i,E \times B}$ and $j_{e,E \times B}$ are simply the opposite of each other, they cannot create net current, but we can see that the calculated magnitude of $j_{E \times B}$ here is larger than the actual value. This deviation is also reflected in the electron results. This deviation can be understood because the accuracy requirement on the electric field is too high for this region. For example, the deviation between $j_{e\perp}$ and $j_{e,E \times B + \text{dia}}$ is about 150 nA/m^2 in region 1. In this region, B is small and $j_{E \times B}$ is sensitive to E . To get this deviation current one just needs an electric field $E \sim 0.9 \text{ mV/m}$. We find that $j_{i,\text{dia}}$ is smaller than $j_{i\perp}$ here, which is different from region 2. This means that the direction of electric field

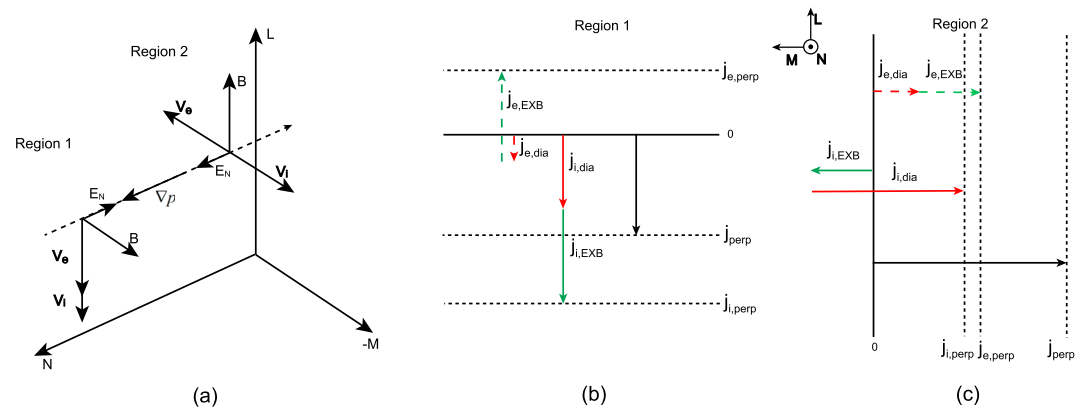


Figure 6. A schematic illustration of the whole process above. (a) The vectors of magnetic field \mathbf{B} , electric field \mathbf{E} , plasma velocity \mathbf{V} , cross-field drift $\mathbf{E} \times \mathbf{B}$, and gradient of pressure ∇p in regions 1 and 2 and (b and c) current distribution in region 1/region 2.

\mathbf{E} in these two regions is different. We can indeed find that E_N in region 1 is negative, while it is positive in region 2 (not shown here).

We can now answer the question: Why do only ions support the perpendicular current in region 1, while both ions and electrons contribute to it in region 2 (Figures 2b–2d)? Actually, most of the current source is $j_{i,dia}$ in both of these two regions, while the different effect of $j_{E \times B}$ in each region adds to the separated portions of ion and electron currents differently in each region. The electric field does not produce any total current but simply redistributes the current density between ions and electrons. We can describe all the above process clearly from the schematic illustration below.

Figure 6a shows all the vectors in regions 1 and 2. For this simplified schematic, we assume that magnetic field is always in the $-M$ direction and the electric field is in the $-N$ direction in region 1. An important feature is that both electrons and ions are moving along the $-L$ direction. This result is consistent with the particle-in-cell simulations of (Voitcu & Echim, 2017), which suggested that the tangential deflection is charge independent when the MSH jet meets the tangential discontinuity type MP. The reason is that cross-field drift plays a major role in this region. The gradient of ion pressure, ∇p_i , always exists in region 1 even though region 1 is in the MSH. The $j_{i,dia}$ caused by this gradient is the source of current in region 1 (Figure 6b). The ion current is larger than $j_{i,dia}$ because $j_{i,E \times B}$ is in the same direction with $j_{i,dia}$ here. The electron current is dominated by $j_{e,E \times B}$ so its direction is opposite to the ion current.

In region 2, the magnetic field is mainly in the $+L$ direction and electric field points in the $+N$ direction. Electrons and ions are moving in opposite senses in the M direction (Figure 6a). This is clearly different from region 1, and we suggest this means that the effect of the diamagnetic drift is more important than the cross-field drift in this region. This is also reflected in the current structure in Figure 6c.

2.4. Non-MHD Effect of Ions

In the above event, both ions and electrons can almost be described with MHD theory because the calculated, combined, $j_{E \times B + dia}$ is consistent with j_{\perp} . This is plausible since the MP thickness is a little larger than the ion gyroradius. Nevertheless, the detailed behavior of the currents (electrons in particular) reveals effects which are not part of the classical Chapman-Ferraro model. We therefore have investigated other events to find examples of MP structure which cannot be described by MHD theory. We give one example in Figure 7. From the reversal of tangential magnetic field features (Figure 7a), we find that this is also a typical MP crossing case. MMS initially stays in the MSP then crosses the MP and enters into the MSH. During this MP crossing, the radial separation of the electron and ion edge can be observed (not shown here). This indicates that spacecraft crossed an open/closed magnetic field boundary layer created by magnetic reconnection (Gosling et al., 1990). The absence of a large electric field and plasma heating, however, indicates that the crossing is not located within the reconnection region but lies somewhat downstream of it. We also calculate each of the terms of equation (2) similarly to Figure 6, and the

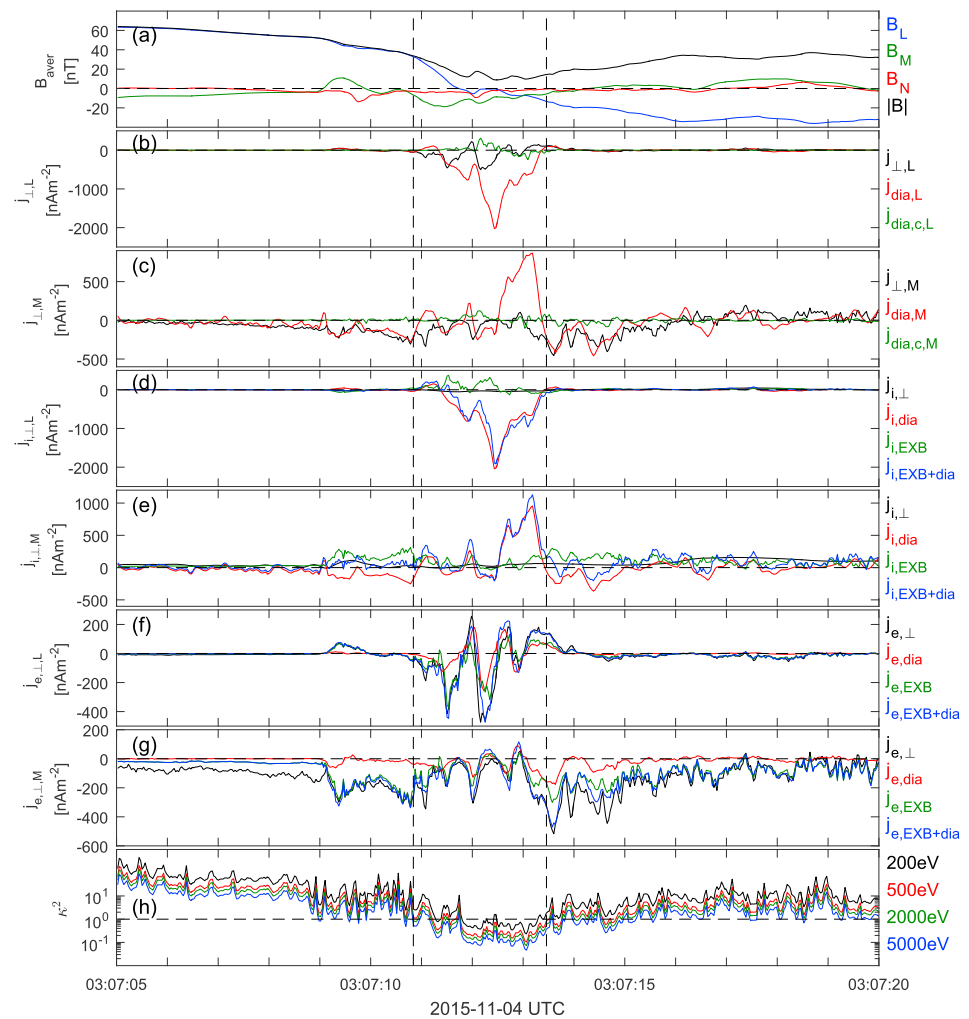


Figure 7. All the calculated terms in equation (2) on 4 November 2015. (a) Four spacecraft average magnetic field; (b and c) perpendicular current from four spacecraft plasma moments j_{\perp} (black), diamagnetic drift current j_{dia} (red), and curvature drift current $j_{\text{dia},c}$ (green); (d–g) ion/electron perpendicular current (black), diamagnetic drift current (red), cross-field drift current (green), sum of diamagnetic drift current, and cross-field drift current (blue); (h) the adiabatic parameter κ^2 for four different ion energies based on the results of a magnetic curvature analysis.

results are shown in Figures 7b–7g. We define a region between two vertical dashed lines: j_{dia} is almost consistent with j_{\perp} outside this region (Figures 7b and 7c). Within the region, however, we find that the calculated j_{dia} is much larger than j_{\perp} . This means that MHD theory cannot be used. For the ions, $j_{i,E \times B + \text{dia}}$ is indeed not consistent with $j_{i,\perp}$ (Figures 7d and 7e). For the electrons, $j_{e,E \times B + \text{dia}}$ is consistent with $j_{e,\perp}$ (Figures 7f and 7g). It indicates that the ions are demagnetized and do not satisfy MHD assumption while electrons appear to satisfy the MHD theory. It needs to be mentioned that $j_{e,\text{dia}}$ can contribute up to 45% of $j_{e,\perp}$ during some intervals between the two dashed lines (Figures 7f and 7g).

In this event, the calculated overall current layer thickness from the timing method is ~ 560 km, and this is much larger than the ion gyroradius. In order to find why the ions do not satisfy MHD theory, we calculate the adiabatic parameter κ^2 defined by the square of the ratio curvature radius / gyroradius (Figure 7h) and track this across the event. Based on this parameter, theory predicts that particles will be nonadiabatic when κ^2 is close to or smaller than one gyroradius (Büchner & Zelenyi, 1989). We can indeed find that κ^2 for ions is close to or much smaller than 1 within the region between the two dashed lines, suggesting that the current layer splits into small substructure in this case. The $j_{\text{dia},c}$ is also not very large here, even though the R_c is small (Figures 7b and 7c), and this may result from the small pressure anisotropy.

This event therefore suggests that whether an MP current layer can be described with MHD theory does not depend on the thickness of the whole current layer because some small substructures may be present in the MP even if the whole thickness is much larger than the gyroradius. Above all, the adiabatic parameter κ^2 is a method to predict the relevant spatial scales of the MP, and this parameter was always large in the previous event. Comparing the calculated $j_{E \times B + dia}$ with j_{\perp} can also be a good way to check if a MP is an MHD one.

3. Discussion and Conclusions

In conclusion, we have investigated current carriers and current sources of an ion scale tangential type MP current layer. During this MP current layer, ions and electrons contribute comparable perpendicular current, while electrons contribute all the parallel current. The energy range of all these current carriers is from middle to high (>100 eV). Particles with high energy have more efficiency to create current. Two-fluid MHD theory under stationary conditions is used to describe the current sources. We find that the diamagnetic current is the source of perpendicular current, with the ion diamagnetic current being dominant (85%). Under the redistribution of the electric field, ions and electrons ultimately carry comparable current.

It is clear from Figure 5 that current exists in both regions 1 and 2. For region 1, the velocity of ions and electrons are different, and this different motion of ions and electrons creates a current. From MHD theory, the source of this current is the ion diamagnetic current (Figures 5d and 5e), which means that the ion pressure gradient exists not only in MP current layer (region 2) but also in the region immediately upstream. This pressure gradient cannot be observed clearly by single spacecraft (Figure 1d) but is revealed here with the multispacecraft measurements.

Although the partial electron and ion perpendicular currents show distinct effects changing from regions 1 to 2, it is found that the ion diamagnetic current is always the main current source of the total perpendicular current. The changing behavior illustrates the importance of the electric field, which plays a key role in redistributing the ion and electron currents. Thus, different proportions of ion and electron currents which evolve through the MP current layer can be a very common feature of the MP current layer, although the ion pressure gradient is often larger than the electron pressure gradient because the ion pressure is usually an order of magnitude greater than electron pressure. The details of the electron and ion response therefore show effects beyond the classic Chapman-Ferraro model.

Since the first event has a simple structure and an overall spatial scale of order the ion gyroradius, the curvature current is small compared to the diamagnetic current at the MP current layer. If the pressure anisotropy and magnetic field are fixed, large curvature current means small curvature radius. However, small curvature radius may violate the MHD assumption so that the curvature current cannot be used because it is a concept of MHD theory. Thus, we predict that small curvature current at the MP current layer is a common condition. We note here that this is different from the magnetotail current sheet. In the magnetotail, the curvature current is usually an important part of current source (e.g., Zelenyi et al., 2010). This could be due to the small pressure gradient in the magnetotail.

In addition to the perpendicular response, a large parallel current exists in this MP current layer. This parallel current is carried by electrons due to the low mass of electron. By comparing parallel and perpendicular electron current carriers, we can see that their energy range is similar (100–400 eV; Figures 3d and 4f and 4g). This may indicate that parallel current is created by a twisted magnetic field which transfers perpendicular current into the parallel component.

We also show another event in which ions are demagnetized and do not satisfy MHD theory while electrons do (the predicted ion MHD current is not consistent with plasma current, while the electron current results match well). We find that the small-scale adiabatic parameter (curvature radius/gyroradius) during this region supports our opinion that this second event contains small-scale substructure and therefore suggests that, whether a MP current layer can be described with MHD theory or not does not depend on the thickness of the whole current layer because small substructures may develop even when the boundary layer thickness is much larger than the gyroradius. The parameter can well predict whether the MHD theory can be used when the total MP thickness is larger than ion gyroradius, but substructure exists within the current layer. The physical mechanism of these substructures needs to be further investigated in the future. In this case, electron diamagnetic current can contribute up to 45% of total perpendicular current during some

intervals between the two dashed lines. This may be due to the ion current being disrupted and could be initiated by demagnetized ions.

Finally, we suggest that calculating each current term from two-fluid MHD theory can be used to analyze the physics of the current layer, particularly given the high precision MMS data. Comparing the predicted MHD current with plasma current can be a good method to judge whether MHD theory is satisfied for electrons or ions in each specific circumstance. In this paper, we show a thin current layer event in which ions and electrons are magnetized, current is dominated by ion diamagnetic drift, while curvature drift can be neglected. We also show another normal thickness current layer while ions are demagnetized in some region for comparison. In order to get more general physical conclusions for the MP current layer, more events and statistical study are needed in the future.

Acknowledgments

For MMS data visit <https://lasp.colorado.edu/mms/sdc/public/>. We thank the entire MMS team and instrument PIs for data access and support. M. W. Dunlop is partly supported by an STFC in-house research grant and is supported by the NSFC grants 41574155 and 41431071. This work is partly supported through an ISSI Team “from cluster to MMS.” We thank the International Space Science Institute in Bern, Switzerland; its staff; and directors.

References

- Baumjohann, W., & Treumann, R. (1997). *Basic space plasma physics* (p. 147). London: Imperial College Press.
- Berchem, J., & Russell, C. T. (1982). The thickness of the magnetopause current layer: ISEE 1 and 2 observations. *Journal of Geophysical Research*, *87*(A4), 2108–2114. <https://doi.org/10.1029/JA087iA04p02108>
- Büchner, J., & Zelenyi, L. M. (1989). Regular and chaotic charged particle motion in magnetotail like field reversals: 1. Basic theory of trapped motion. *Journal of Geophysical Research*, *94*(A9), 11821–11,842. <https://doi.org/10.1029/JA094iA09p11821>
- Burch, J. L., Moore, T. E., Torbert, R. B., & Giles, B. L. (2015). Magnetospheric Multiscale overview and science objectives. *Space Science Reviews*, *199*(1–4), 5–21. <https://doi.org/10.1007/s11214-015-0164-9>
- Chapman, S., & Ferraro, V. C. A. (1930). A new theory of magnetic storms. *Nature*, *126*(3169), 129–130. <https://doi.org/10.1038/126129a0>
- Dong, X.-C., Dunlop, M. W., Trattner, K. J., Phan, T. D., Fu, H. S., Cao, J. B., et al. (2017). Structure and evolution of flux transfer events near dayside magnetic reconnection dissipation region: MMS observations. *Geophysical Research Letters*, *44*, 5951–5959. <https://doi.org/10.1002/2017GL073411>
- Dunlop, M. W., & Balogh, A. (2005). Magnetopause current as seen by Cluster. *Annales de Geophysique*, *23*(3), 901–907. <https://doi.org/10.5194/angeo-23-901-2005>
- Dunlop, M. W., Balogh, A., & Glassmeier, K.-H. (2002). Four-point Cluster application of magnetic field analysis tools: The discontinuity analyzer. *Journal of Geophysical Research*, *107*(A11), 1385. <https://doi.org/10.1029/2001JA005089>
- Dunlop, M. W., Haaland, S., Escoubet, P. C., & Dong, X.-C. (2016). Commentary on accessing 3-D currents in space: Experiences from Cluster. *Journal of Geophysical Research: Space Physics*, *121*, 7881–7886. <https://doi.org/10.1002/2016JA022668>
- Dunlop, M. W., Zhang, Q.-H., Bogdanova, Y. V., Lockwood, M., Pu, Z., Hasegawa, H., et al. (2011). Extended magnetic reconnection across the dayside magnetopause. *Physics Review Letters*, *107*, 025004. <https://doi.org/10.1103/PhysRevLett.107.025004>
- Gosling, J. T., Thomsen, M. F., Bame, S. J., Onsager, T. G., & Russell, C. T. (1990). The electron edge of low latitude boundary layer during accelerated flow events. *Geophysical Research Letters*, *17*(11), 1833–1836. <https://doi.org/10.1029/GL017i011p01833>
- Haaland, S., Reistad, J., Tenfjord, P., Gjerloev, J., Maes, L., DeKeyser, J., et al. (2014). Characteristics of the flank magnetopause: Cluster observations. *Journal of Geophysical Research: Space Physics*, *119*, 9019–9037. <https://doi.org/10.1002/2014JA020539>
- Haaland, S., Sonnerup, B. U. Ö., Dunlop, M. W., Georgescu, E., Paschmann, G., Klecker, B., & Vaivads, A. (2004). Orientation and motion of a discontinuity from Cluster curlometer capability: Minimum variance of current density. *Geophysical Research Letters*, *31*, L10804. <https://doi.org/10.1029/2004GL020001>
- Le, G., & Russell, C. T. (1994). The thickness and structure of high beta magnetopause current layer. *Geophysical Research Letters*, *21*(23), 2451–2454. <https://doi.org/10.1029/94GL02292>
- Lindqvist, P.-A., Olsson, G., Torbert, R. B., King, B., Granoff, M., Rau, D., et al. (2016). The spin-plane double probe electric field instrument for MMS. *Space Science Reviews*, *199*(1–4), 137–165. <https://doi.org/10.1007/s11214-014-0116-9>
- Panov, E. V., Artemyev, A. V., Nakamura, R., & Baumjohann, W. (2011). Two types of tangential magnetopause current sheets: Cluster observations and theory. *Journal of Geophysical Research*, *116*, A12204. <https://doi.org/10.1029/2011JA016860>
- Paschmann, G., & Schwartz, S. J. (2000). *ISSI book on analysis methods for multi-spacecraft data*, ESA spec. Publ., (Vol. 449). Bern, Switz: Int. space Sci. Inst.
- Phan, T. D., Dunlop, M. W., Paschmann, G., Klecker, B., Bosqued, J. M., Rème, H., et al. (2004). Cluster observations of continuous reconnection at the magnetopause under steady interplanetary magnetic field conditions. *Annales de Geophysique*, *22*(7), 2355–2367. <https://doi.org/10.5194/angeo-22-2355-2004>
- Phan, T. D., Gosling, J. T., Paschmann, G., Pasma, C., Drake, J. F., Øieroset, M., et al. (2010). The dependence of magnetic reconnection on plasma β and magnetic shear: Evidence from solar wind observations. *The Astrophysical Journal Letters*, *719*(2), L199.
- Pollock, C., Moore, T., Jacques, A., Burch, J., Gliese, U., Saito, Y., et al. (2016). Fast plasma investigation for Magnetospheric Multiscale. *Space Science Reviews*, *199*(1–4), 331–406. <https://doi.org/10.1007/s11214-016-0245-4>
- Russell, C. T., Anderson, B. J., Baumjohann, W., Bromund, K. R., Dearborn, D., Fischer, D., et al. (2016). The Magnetospheric Multiscale magnetometers. *Space Science Reviews*, *199*(1–4), 189–256. <https://doi.org/10.1007/s11214-014-0057-3>
- Shen, C., Li, X., Dunlop, M., Liu, Z. X., Balogh, A., Baker, D. N., et al. (2003). Analyses on the geometrical structure of magnetic field in the current sheet based on cluster measurements. *Journal of Geophysical Research*, *108*(A5), 1168. <https://doi.org/10.1029/2002JA009612>
- Trenchi, L., Marcucci, M. F., Palocchia, G., Consolini, G., Bavassano Cattaneo, M. B., di Lellis, A. M., et al. (2008). Occurrence of reconnection jets at the dayside magnetopause: Double Star observations. *Journal of Geophysical Research*, *113*, A07510. <https://doi.org/10.1029/2007JA012774>
- Voitcu, G., & Echim, M. (2017). Tangential deflection and formation of counterstreaming flows at the impact of a plasma jet on a tangential discontinuity. *Geophysical Research Letters*, *44*, 5920–5927. <https://doi.org/10.1002/2017GL073763>
- Zelenyi, L. M., Artemyev, A. V., Malova, K. V., Petrukovich, A. A., & Nakamura, R. (2010). Metastability of current sheets. *Physics-Uspekhi*, *53*(9), 933–941. <https://doi.org/10.3367/UFNe.0180.201009g.0973>